An Introduction to EEG Source Analysis with an illustration of a study on Error-Related Potentials

Marco Congedo, Sandra Rousseau, Christian Jutten

Guide to Brain-Computer Music Interfacing, edited by Eduardo Reck Miranda, Julien Castet and Benjanim Knapp, Springer, London

CHAPTER 8 - An Introduction to EEG Source Analysis with an illustration of a study on Error-Related Potentials.

Marco Congedo, Sandra Rousseau, Christian Jutten*

GIPSA-lab, CNRS and Grenoble University, Grenoble, FRANCE

* Corresponding Author

Address :

11 rue des Mathématiques, Domaine universitaire - BP 46 - 38402, Grenoble, France.

E-mail : marco.congedo@gmail.com

8.1 Introduction

Over the last twenty years blind source separation (BSS) has become a fundamental signal processing tool in the study of human electroencephalography (EEG), other biological data, as well as in many other signal processing domains such as speech, images, geophysics and wireless communication (Comon and Jutten, 2010). Without relying on head modeling BSS aims at estimating both the waveform and the scalp spatial pattern of the intracranial dipolar current responsible of the observed EEG, increasing the sensitivity and specificity of the signal received from the electrodes on the scalp. This chapter begins with a short review of brain volume conduction theory, demonstrating that BSS modeling is grounded on current physiological knowledge. We then illustrate a general BSS scheme requiring the estimation of second-order statistics (SOS) only. A simple and efficient implementation based on the approximate joint diagonalization of covariance matrices (AJDC) is described. The method operates in the same way in the time or frequency domain (or both at the same time) and is capable of modeling explicitly physiological and experimental source of variations with remarkable flexibility. Finally, we provide a specific example illustrating the analysis of a new experimental study on error-related potentials.

The AJDC method for EEG data has been reviewed and described in details in Congedo et al. (2008), based upon theoretical bases to be found in Pham (2002) and Pham and Cardoso (2001). Typically, it has been used on continuously recorded EEG (*spontaneous activity*: e.g., Van der Loo et al., 2007). An extension of the method to treat group EEG data and normative EEG data has been proposed in Congedo et al. (2010). Such group BSS approach has been used in a clinical study on obsessive-compulsive disorder in Kopřivová et al. (2011) and in a cognitive study on spatial navigation in White et al. (2012). The AJDC method has also been employed for motor imagery-based brain-computer interfaces in Gouy-Pailler et al. (2010), showing that it can be applied purposefully to event-related (de)synchronization data (*induced activity*). Extensions of the method to the analysis of simultaneous multiple-subject EEG data is a current line of research in our laboratory (Chatel-Goldman, Congedo and Phlypo, 2013; Congedo, Phlypo and Pham, 2011; Congedo, Phlypo and Chatel-Goldman, 2012). This chapter contributes demonstrating that the AJDC method can be used purposefully on event-related potential (ERP) data as well (*evoked activity*).

8.2 Physiological ground of BSS modeling

It is well established that the generators of brain electric fields recordable from the scalp are macroscopic post-synaptic potentials created by assemblies of pyramidal cells of the neocortex (Speckmann and Elger, 2005). Pyramidal cells are aligned and oriented perpendicularly to the cortical surface. Their synchrony is possible thanks to a dense net of local horizontal connections (mostly <1mm). At recording distances larger than about three/four times the diameter of the synchronized assemblies the resulting potential behaves as if it were produced by electric dipoles; all higher terms of the multipole expansion vanish and we obtain the often invoked dipole approximation (Lopes Da Silva and Van Rotterdam,

2005; Nunez and Srinivasan, 2006, Ch. 3). Three physical phenomena are important for the arguments we advocate in this study. First, unless dipoles are moving there is no appreciable delay in the scalp sensor measurement (Lopes da Silva and Van Rotterdam, 2005). Second, in brain electric fields there is no appreciable electro-magnetic coupling (magnetic induction) in the frequencies up to about 1MHz, thus the quasi-static approximation of Maxwell equations holds throughout the spectrum of interest (Nunez and Srinivasan, 2006, p. 535-540). Finally, for source oscillations below 40Hz it has been verified experimentally that capacitive effects are also negligible, implying that potential difference is in phase with the corresponding generator (Nunez and Srinivasan, 2006, p. 61). These phenomena strongly support the *superposition principle*, according to which the relation between neocortical dipolar fields and scalp potentials may be approximated by a system of linear equations (Sarvas, 1987). We can therefore employ a *linear BSS model*. Because of these properties of volume conduction, scalp EEG potentials describe an *instantaneous mixture* of the fields emitted by several dipoles extending over large cortical areas. Whether this is a great simplification, we need to keep in mind that it does not hold true for all cerebral phenomena. Rather, it does at the macroscopic spatial scale concerned by EEG.

The goal of EEG blind source separation (BSS) is to "isolate" in space and time the generators of the observed EEG as much as possible, counteracting the mixing caused by volume conduction and maximizing the signal-to-noise ratio (SNR). First explored in our laboratory during the first half of the 80's (Ans et al., 1985; Hérault and Jutten, 1986), BSS has enjoyed considerable interest worldwide only starting a decade later, inspired by the seminal papers of Jutten and Hérault (1991), Comon (1994) and Bell and Sejnowski (1995). Thanks to its flexibility and power BSS has today greatly expanded encompassing a wide range of applications such as speech enhancement, image processing, geophysical data analysis, wireless communication and biological signal analysis (Comon and Jutten, 2010).

8.3 The BSS problem for EEG, ERS/ERD and ERP

For N scalp sensors and $M \leq N$ EEG dipolar fields with fixed location and orientation in the analyzed time interval, the linear BSS model simply states the superposition principle discussed above, i.e.,

$$\boldsymbol{v}(t) = \boldsymbol{A}\boldsymbol{s}(t) + \boldsymbol{\eta}(t) \qquad (8.1)$$

$\boldsymbol{v}(t) \in \Re^N$ is the *sensor measurement vector* at sample t, $\boldsymbol{A} \in \Re^{N \cdot M}$ is a time-invariant full column rank *mixing matrix*, $\boldsymbol{s}(t) \in \Re^M$ holds the time-course of the source components and $\boldsymbol{\eta}(t) \in \Re^N$ is additive noise, temporally white, possibly uncorrelated to $\boldsymbol{s}(t)$ and with spatially uncorrelated components. Equation (8.1) states that each observation $\boldsymbol{v}(t)$ (EEG) is a linear combination (mixing) of sources $\boldsymbol{s}(t)$, given by the coefficients in the corresponding column of matrix $\boldsymbol{A}$. Neither $\boldsymbol{s}(t)$ nor $\boldsymbol{A}$ are known, that is why the problem is said to be *blind*. Our source estimation is given by

$$\hat{\boldsymbol{s}}(t) = \hat{\boldsymbol{B}}\boldsymbol{v}(t) \qquad (8.2)$$

where $\boldsymbol{B} \in \Re^{M \cdot N}$ is called the *demixing* or *separating matrix*. This is what we want to estimate in order to recover the sources from EEG. Hereafter the hat indicates a statistical estimation. Although this is the classical BSS model we need a few clarifications for the EEG case: by $\boldsymbol{\eta}(t)$ we model *instrumental* noise only. In the following we drop the $\boldsymbol{\eta}(t)$ term because the instrumental (and quantization) noise of modern EEG equipment is typically low (<1μV). On the other hand, *biological* noise (extra-cerebral artifacts such as eye movements and facial muscle contractions) and *environmental* noise (external electromagnetic interference) may obey a mixing process as well, thus they are generally modeled as components of $\boldsymbol{s}(t)$, along with cerebral ones. Notice that while biological and environmental noise can be identified as separated components of $\boldsymbol{s}(t)$, hence removed, source estimation will be affected by the underlying cerebral *background noise* propagating with the same coefficients as the signal (Belouchrani and Amin, 1998).

8.4 A suitable class of solutions to the brain BSS problem

To tackle problem (8.2) assuming knowledge of sensor measurement only we need to reduce the number of admissible solutions. In this paper we are interested in weak restrictions converging toward condition

$$\hat{\boldsymbol{s}}(t) = \boldsymbol{G}\boldsymbol{s}(t), \qquad (8.3)$$

where $\boldsymbol{s}(t)$ holds the time-course of the true (unknown) source processes, $\hat{\boldsymbol{s}}(t)$ our estimation and the *system matrix*

$$\boldsymbol{G} = \hat{\boldsymbol{B}}\boldsymbol{A} \approx \boldsymbol{\Lambda}\boldsymbol{P} \qquad (8.4)$$

approximates a signed scaling (a diagonal matrix $\boldsymbol{\Lambda}$) and permutation ($\boldsymbol{P}$) of the rows of $\boldsymbol{s}(t)$. Equation (8.3) is obtained by substituting (8.1) in (8.2) ignoring the noise term in the former. Whether condition (8.3) may be satisfied is a problem of *identifiability*, which establishes the theoretical ground of BSS theory (Tong, Inouye and Liu, 1993; Cardoso, 1998; Pham and Cardoso, 2001; Pham, 2002). We will come back on how identifiability is sought in practice with the proposed BSS approach. Matching condition (8.3) implies that we can recover faithfully the source *waveform*, but only out of a *scale* (including sign) and *permutation* (order) indeterminacy. This limitation is not constraining for EEG, since it is indeed the waveform that bears meaningful physiological and clinical information. Notice the correspondence between the m^{th} source, its *separating vector* (m^{th} *row* of $\hat{\boldsymbol{B}}$) and its *scalp spatial pattern* (mixing vector), given by the m^{th} *column* of $\hat{\boldsymbol{A}} = \hat{\boldsymbol{B}}^{+}$. Hereafter superscript + indicates the Moore-Penrose pseudo-inverse. The mono-dimensionality of those vectors and their sign/energy indeterminacy implies the explicit modeling of the orientation and localization parameters of the m^{th} source, but not its moment. This is also the case of inverse solutions with good source localization performance (Greenblatt et al., 2005). On the other

hand, when we estimate current density by EEG inverse solutions we estimate current flowing in the three orthogonal directions (hence the filter is given by three vectors, not one as here), resulting in a considerable loss of spatial resolution. Linearity allows switching back from the source space into the sensor space. Substituting (8.2) into (8.1) and dropping the noise term in the latter yields *BSS filtering*

$$\boldsymbol{v}'(t) = \hat{\boldsymbol{A}}\boldsymbol{R}\hat{\boldsymbol{s}}(t) = \hat{\boldsymbol{A}}\boldsymbol{R}\hat{\boldsymbol{B}}\boldsymbol{v}(t)\,,$$

where $\boldsymbol{R}$ is a diagonal matrix with m^{th} diagonal element equal to 1 if the m^{th} component is to be retained and equal to 0 if it is to be removed. BSS filtering is common practice to remove artifacts from the EEG data.

8.5 An approach for solving the BSS problem based on second-order statistics only

It has been known for a long time that in general the BSS problem cannot be solved for sources that are Gaussian, independent and identically distributed (iid) (Darmois, 1953). EEG data is clearly non-iid, thus we may proceed assuming that source components are all pair-wise uncorrelated and that either (a) within each source component the successive samples are temporally correlated[1], (Molgedey and Schuster, 1994; Belouchrani et al., 1997) or (b) samples in successive time intervals do not have the same statistical distribution, i.e., they are non stationary (Matsuoka et al., 1995; Souloumiac, 1995; Pham and Cardoso, 2001). Provided that *source components have non-proportional spectra or the time courses of their variance (energy) vary differently*, one can show that SOS are sufficient for solving the source separation problem (Yeredor, 2010). Since SOS are sufficient, the method is able to separate also Gaussian sources, contrary to another well known BSS approach named *independent component analysis* (ICA: Comon and Jutten, 2010). If these assumptions are fulfilled the separating matrix can be identified uniquely, thus source can be recovered *regardless the true mixing process* (uniform performance property: see for example Cardoso, 1998) and regardless the distribution of sources, which is a remarkable theoretical advantage. The fundamental question is therefore whether or not the above assumptions fits EEG, ERS/ERD and ERP data.

- **Sources are uncorrelated:** This assumption may be conceived as a working assumption. In practice, the BSS output is never exactly uncorrelated, but just as uncorrelated as possible. What we try to estimate is the coherent signal of large cortical patches, enough separated in space one from the other. BSS may be conceived as a spatial filter minimizing the correlation of the observed mixtures and recovering the signal emitted from the most energetic and uncorrelated cortical patches. For EEG data this is an effective way to counteract the effect of volume conduction. In fact, we have seen that the brain tissue behaves approximately as a linear conductor, thus observed potentials (mixtures) must be more correlated than the generating dipolar fields.

[1] Such processes are called *colored*, in opposition to iid processes, which are called *white*.

- **Sources are colored and/or their energy varies over time:** Observed potentials are the summation of post-synaptic potentials over large cortical areas caused by trains of action potentials carried by afferent fibers. The action potentials come in trains/rest periods, resulting in sinusoidal oscillations of the scalp potentials, with negative shifts during the train discharges and positive shifts during rest. The periodicity of trains/rest periods are deemed responsible for high-amplitude EEG rhythms (oscillations) up to about 12Hz, whereas higher frequency (>12Hz) low-amplitude rhythms may result from sustained (tonic) afferent discharges (Speckmann and Elegr, 2005). There is no doubt that an important portion of spontaneous EEG activity is rhythmic, whence strongly colored (Niedermeyer, 2005 a; Steriade, 2005; Buzsáki, 2006, Ch. 6, 7). Some rhythmic waves come in more or less short bursts. Typical examples are sleep spindles (7-14Hz) (Niedermeyer, 2005 b; Steriade, 2005), frontal Theta (4-7Hz) and Beta (13-35Hz) waves (Niedermeyer, 2005 a). Others are more sustained, as it is the case for slow Delta (1-2Hz) waves during deep sleep stages III and IV (Niedermeyer, 2005 b), the Rolandic Mu rhythms (around 10Hz and 20Hz) and posterior Alpha rhythms (8-12Hz) (Niedermeyer, 2005 a). In all cases brain electric oscillations are not ever-lasting and one can always define time intervals when rhythmic activity is present and others when it is absent or substantially reduced. Such intervals may be precisely defined based on known reactivity properties of the rhythms. For example, in event-related synchronization / desynchronization (ERD/ERS: Pfurtscheller and Lopes da Silva, 2004), which are time locked, but not phase locked increases and decreases of the oscillating energy (Steriade, 2005) intervals may be defined before and after event onset. On the other hand event-related potentials (ERP: Lopes Da Silva, 2005 b), which are both time-locked and phase-locked can be further partitioned in several successive intervals comprising the different peaks. Such source energy variation signatures can be modeled precisely by SOS, as we will show with the ensuing ErrP study.

8.6 Approximate joint diagonalization of covariance matrices (AJDC)

The SOS BSS method we are considering is consistently solved by *approximate joint diagonalization* algorithms (Cardoso and Souloumiac[2], 1993; Tichavsky and Yeredor, 2009). Given a set of covariance matrices $\{\boldsymbol{C}_{1,}\ \boldsymbol{C}_{2,}\ldots\}$, the AJD seeks a matrix $\hat{\boldsymbol{B}}$ such that the products $\hat{\boldsymbol{B}}\boldsymbol{C}_1\hat{\boldsymbol{B}}^T$, $\hat{\boldsymbol{B}}\boldsymbol{C}_2\hat{\boldsymbol{B}}^T$, … are as diagonal as possible (subscript "T" indicates matrix transposition). Given an appropriate choice of the *diagonalization set* $\{\boldsymbol{C}_{1,}\ \boldsymbol{C}_{2,}\ldots\}$ such matrix $\hat{\boldsymbol{B}}$ is indeed an estimation of the separating matrix in (8.2) and one obtains an estimate of the mixing matrix as $\hat{\boldsymbol{A}}=\hat{\boldsymbol{B}}^{+}$. Matrices in $\{\boldsymbol{C}_{1,}\ \boldsymbol{C}_{2,}\ldots\}$ are chosen so as to hold in the off-diagonal entries statistics describing some form of *correlation* among the sensor measurement

[2] This paper does not consider SOS but 4th order statistics, however, the algorithms is based on approximate joint diagonalisation of matrices which are the slices of the tensor of 4th order cumulants, thus can be used for SOS matrices as well.

channels; then the AJD will vanish those terms resulting in linear combination vectors (the rows of $\hat{\boldsymbol{B}}$) extracting uncorrelated components from the observed mixture via (8.2). More particularly, the joint diagonalization is applied on matrices that *change* according to the assumptions about the source. They are those changes, when available, that provide enough information to solve the BSS problem. Formally, for AJDC the identifiability of sources discussed above, that is, matching condition (8.3), is described by the fundamental AJD-based BSS theorem (Afsari, 2008; see also Aïssa-El-Bey et al., 2008): let matrices $\boldsymbol{S}_1$, $\boldsymbol{S}_2$,.. be the K (unknown) covariance matrices of sources corresponding to the covariance matrices included in the diagonalization set and $\boldsymbol{s}_{k(ij)}$ their elements. The diagonal elements of these matrices $\boldsymbol{s}_{k(ii)}$ hold the source variance. The off-diagonal elements $\boldsymbol{s}_{k(ij),\ i\neq j}$, are null as sources are assumed to be uncorrelated. Let

$$\boldsymbol{Y} = \left(\boldsymbol{y}_1 \cdots \boldsymbol{y}_M\right)^T = \begin{pmatrix} s_{1(11)} & \cdots & s_{k(11)} \\ \vdots & \ddots & \vdots \\ s_{1(MM)} & \cdots & s_{k(MM)} \end{pmatrix} \quad (8.5)$$

be the matrix formed by stacking one below the other row vectors $\boldsymbol{y}_1, \boldsymbol{y}_2, \ldots \boldsymbol{y}_M$ constructed as shown in Fig. 8.1. Each vector $\boldsymbol{y}_m=(s_{1(mm)},\ldots,s_{K(mm)})$ holds the *energy profile along the diagonalization set* for each source, with m:1…M and M the number of estimated sources. *The fundamental theorem says that the m^{th} source can be separated as long as its energy profile vector $\boldsymbol{y}_m$ is not collinear* [3] *with any other vector in* $\boldsymbol{Y}$. Said differently, the wider the angle between $\boldsymbol{y}_m$ and any other vector in $\boldsymbol{Y}$, the greater the chance to separate the m^{th} source. Even if two vectors are collinear, the other sources can still be identified.

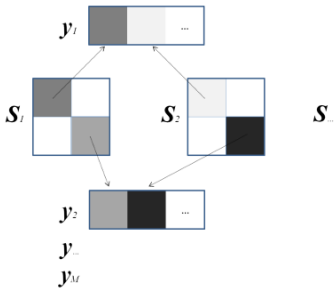

Figure 8.1: Graphical illustration of the construction of the source energy profile vectors $\boldsymbol{y}_m$.

Table 8.1 reports useful information to define an appropriate diagonalization set so as to ensure identifiability of sources.

[3] Two vectors are collinear if they are equal out of a scaling factor, that is, the energy profile is proportional.

Table 8.1: Criteria to achieve identifiability of sources in BSS methods based on AJD of SOS.

Assumption on the sources	**Covariance Matrices (CM) Estimation**	**What is the energy profile**	**Sufficient condition for Identifiability**	**Examples of data**
Coloration	*i.* Lagged Covariance matrices, *ii.* Fourier Co-spectral Matrices, *iii.* CM estimated with a filter bank	*i.* The source *autocorrelation*, *ii.* The source *power spectrum* *iii.* as in *ii.*	The power spectrum of the source is non-proportional to the power spectrum of any other sources	Spontaneous oscillation with characteristic power spectrum such as posterior dominant rhythms (Alpha), Somatosensory Mu rhythms, frontal midline Theta, Beta bursts, etc.
Non-Stationary	CM estimated on *j.* different *time blocks* of data *jj.* different *experimental conditions*	The variation of the energy of the source along the *(j) blocks or* *(jj) experimental conditions*	The variation of the source energy along *(j) blocks or (jj) experimental conditions* do not correlate with the same variation of any other sources	- Blocks of data according to physiological reactivity of EEG oscillations (e.g., eyes-close vs. eyes-open) - CM estimated before and after the event in ERD/ERS - CM estimated on different peaks in ERP (after averaging the ERP) - Active vs. Control condition, ...

Importantly, the two basic theoretical frameworks for working in a SOS framework reported in Table 8.1, the *coloration* and the *non-stationary*, can be combined in any reasonable way: one may estimate covariance matrices in different blocks (and/or conditions) for different frequency band-pass regions, effectively increasing the uniqueness of the source energy profile. This is for instance the path we have followed for solving the problem of separating sources generating error potentials, as we will demonstrate here below. In fact, AJDC method can be applied in different representation spaces; applying to (1) any invertible and linearity-preserving transform $\mathcal{T}$ leads to

$$\mathcal{T}\left[\boldsymbol{v}(t)\right] = \boldsymbol{A}\mathcal{T}\left[\boldsymbol{s}(t)\right],$$

which preserves the mixing model. Then, solving source separation in the transformed space still provides estimation of the matrix $\boldsymbol{A}$ or of its inverse $\boldsymbol{B}$, which can be used directly in Eq. (2) for recovering the source $\boldsymbol{s}(t)$ in the initial space. For example, the transform $\mathcal{T}$ may be a discrete Fourier transform, a time-frequency transform such as the Wigner-Ville transform or a wavelet transform. AJDC can be easily and conveniently transposed in the frequency domain, thence in the time-frequency domain, whether we perform the frequency expansion for several time segments.

It is important to consider that the number of matrices should be high enough to help non-collinearity of source energy profiles. One may want to have at least as many matrices in the diagonalization set as sources to be estimated. On the other hand one should not try to increase the number of matrices indefinitely to the detriment of the goodness of their estimation, i.e., selecting too many discrete frequencies or blocks of data that are too shorts. In summary, the key for succeeding with BSS by AJDC is the definition of an adequate size and content of the diagonalization set; it should include matrices estimated on data as homogeneous as possible for each matrix, with enough samples to allow a proper estimation,

in frequency region and time blocks when the signal-to-noise ratio is high and with an high probability to uncover unique source energy profiles.

8.7 A study on Error-related Potentials

We now turn to the illustration of the AJDC method by means of a new study on error-related potentials (ErrP). We show that BSS analysis increases the specificity and sensitivity that can be obtained working at the sensor level, increasing as a consequence the single-trial classification rate. ErrPs are a family of event-related potential (ERP) that can be elicited after the commission of an error, firstly reported in Miltner, Braun and Coles (1997) as associated to receiving external negative feedback after error commission. This feedback error-related potential (ErrPf) is characterized by a negative deflection peaking between 250 and 400 ms with a fronto-central scalp distribution. The authors named it the feedback-related negativity (FRN) and put it in relation with the response error related negativity (ERN) that had been previously reported (Felkenstein et al., 1991; Gehring et al., 1993), also characterized by a negative deflection. Initially the ErrPf has been studied prevalently in the case of gambling tasks with monetary gain and loss. More recently it has attracted much attention in the brain-computer interface (BCI) community because its on-line detection provides a unique opportunity to automatically correct erroneous BCI operations, effectively increasing the consistency and transfer rate of a BCI system (Farquhar and Hill, 2013). In order to do so accurate on-line single-trial ErrP detection is necessary. Here we contribute along this direction in two way: 1) we design a new experimental protocol in order to study single-trial ErrPf detection in a controlled situation that mimics actual BCI operation and 2), we apply the AJDC source analysis in order to better characterize this potential, hence increasing the accuracy of its on-line single-trial detection.

1) New Experimental Protocol

In all previous studies on single-trial detection of ErrP for integration of a control loop in a BCI system the involvement of the participants is very far from the involvement of participants during BCI operation, that is, as such they lack ecological validity. In particular, in previous studies the feedback is the main focus of the subject, while in actual BCI operations receiving such a feedback is only a small part of a complex cognitive task. Furthermore, previous studies have mainly returned shame feedback, that is, feedback completely unrelated to the performance of the subject. Finally, the subject-specific control capability of a BCI system has not been taken into consideration. Here we study the feedback related potential in the case of a memory task, with no monetary gain or loss. The feedback is returned when the subject gives the answer and no reward is given to the subject except a score, thus our participants have no other interest besides their own performance. Such an experimental protocol allows to study the ErrPf in a real "error versus correct" condition. The protocol we use is a memory task inducing a high cognitive load. The subject is continuously

engaged in a demanding task (and not only on the feedback presentation), mimicking the actual conditions of a BCI use, where focus, concentration and attention are essential requisite for successful BCI operation. Then, in this study the feedback corresponds to the actual performance achieved in the task, again approximating the actual operation of a BCI. Finally, the memory task continuously adapts to the ability of the participants during the whole experiment. This ensures that the cognitive load is approximately constant across the duration of the experiment, that it is comparable across individuals regardless of their memory span and that the error rate across subjects is approximately equal. This latter point is particularly important in ErrP studies since it is known that he error rate affects the ErrP ([8]). In this study the adaptive algorithm is tuned to engender an error rate of about 20%, which amount approximately to the reasonable accuracy of a reactive BCI operation in real-world situations.

2) New Multivariate Signal processing Analysis

Some of the previous studies on single trial ErrP classification (correct vs. error) have reached encouraging results (around 70% of overall accuracy) using only little a-priori knowledge on this potential. As usual, a more profound knowledge of the electrophysiological characteristics of the ErrPf can be used to select more relevant and robust features for the purpose of single-trial on line detection. Previous studies showed that the ErrP can be characterized both in the temporal domain as an ERP (time and phase-locked event) and as an event-related synchronization, or ERS (time but non-phase-locked event). The ERP is characterized by a negative deflection, named Ne, sometimes followed by a positive one named Pe (Gentsch, Ullsperger and Ullsperger, 2009; Steinhauser and Kiesel, 2011). The ERS is characterized by an increased oscillatory activity in the theta frequency band-pass region (4-7.5 Hz) occurring approximately in the same time window and spatial location as the Ne (Trujillo and Allen, 2007). Source localization of the FRN using dipole analysis has suggested generators in the anterior cingulate cortex (ACC) and the supplementary motor area (Gehring and Willoughby, 2002; Miltner, Braun and Coles, 1997). Similar results have been obtained for the ErrPr. *Hereby we propose a sharp spatial filtering approach based on the blind source separation approach described above with the aim to disentangling the sources responsible for the ERP and the ERS;* if this proves feasible, then the ERP and ERS components will yield independent features to feed the classifier, hence potentially increasing the on-line accuracy.

As a first objective we identify the different components of the ErrP along dimensions time, space and frequency by means of a multivariate analysis both in the sensor space and in the source space. We jointly estimate the brain sources at the origin of the ERP and ERS components and assess their different role in error reaction. Then we study the role of these components on the ErrP with respect to the expectation of participants. Finally, we look at how these results impact on ErrP single-trial classification, which is the essential step in integrating ErrPs in BCI systems.

8.8 Method

8.8.1 Participants

22 healthy volunteers participated to this experiment. All subjects were BCI-naive at the time of the experiment and none of them reported neurological or psychiatric disorders in their lifetime. Due to the presence of excessive artifacts in the EEG data, three subjects were subsequently excluded from all analyses, leaving 19 participants, of which 9 female and 10 male, with age ranging from 20 to 30 with a mean and a standard deviation of 24 and 2.52, respectively.

8.8.2 Experimental design

The experiment involved two sessions lasting altogether approximately half an hour. Each session consisted of six blocks of six trials, for a total of 6x6x2=72 trials. Participants seated comfortably 80cm in front of a 21-inch computer screen. Nine square boxes were arranged in circle on the screen. Each trial consisted of the same memory retrieval task: the trial started with the display of the current score for 3000ms (initialized at zero) followed by a fixation cross, also displayed for 3000 ms (Fig 8.2a). Then the memorization sequence started; each memorization comprised a random sequence of two to nine digits appearing sequentially in random positions, with each digit of the sequence randomly assigned to a different box for each sequence (Fig 8.2b). Subjects were instructed to retain positions of all digits. At the end of the sequence the target digit (always contained in the previous sequence) was displayed (Fig 8.2c) and subjects had to click with the aid of a mouse on the box where it had appeared. Once the subject had answered, the interface waited for 1500 ms in order to avoid any contamination of ErrP by beta rebound motor phenomena linked to mouse clicking (Pfurtscheller, 1981). Then, if the answer was correct, the chosen box background color turned into green ("correct" feedback), otherwise it turned into red ("error" feedback). Subjects were then asked to report if the feedback (error/correct) matched their expectation by a mouse click (“yes”/ “no”) (Fig 8.2d). Following this answer a random break of 1000 to 1500ms preceded the beginning of the new trial.

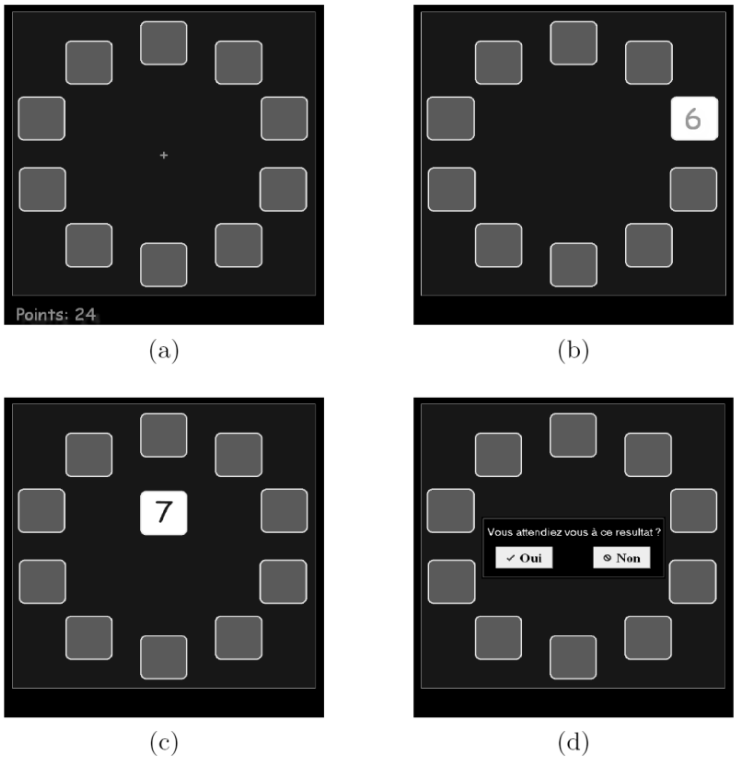

Figure 8.2: Screen shots from the experiment representing different steps of the experiment. a): Fixation cross. b): One digit appearing in the memorization sequence. c): Target digit appearing. d): Feedback report question: 'Vous attendiez-vous à ce resultat' = 'Did you expect this result?', 'Oui'='Yes' and 'Non'='No'.

In order to keep the subjects motivated throughout the experiment, the accumulated score was computed at the beginning of each trial. When subjects localized correctly the target digits their score increased, otherwise, it remained unchanged. The number of digits in the sequence was always between two and nine, fixed within blocks and updated, at the beginning of each block, according to the change in performance from the block just finished and the previous one, as assessed on-line by means of statistical t-tests. The first block started always with four digits for all subjects. The parameters of the adaptation were set thanks to a pilot study and a computer simulation and were chosen to yield about 20% of errors, regardless the working memory ability. Moreover, our learning approach is capable of adapting to fatigue as well as other possible nuisance intervening during the experiment. A random rest break was allowed between blocks, during which the boxes performed a colorful animation chosen each time at random among four preset animations. Between the two sessions the screen was shut down to allow a rest break of 2 - 3 minutes.

8.8.3 Data Acquisition

EEG recordings were acquired from 31 silver/chloride electrodes positioned according to the extended 10/20 system (FP1, FPz, FP2, F7, F3, Fz, F4, F8, FT7, FC3, FCz, FC4, FT8, T7, C3, Cz, C4, T8, TP7, CP3, CPz, CP4, TP8, P7, P3, Pz, P4, P8, O1, Oz, O2) with the aid of a standard elastic cap. Both earlobes, digitally linked, were used as electrical reference. The

ground sensor was positioned on the forehead. The impedance of each sensor was kept below 5k. The EEG was band-pass filtered in the range 0.1-70 Hz and digitized at 500 Hz using the Mitsar 202 DC EEG acquisition system (Mitsar Co. Ltd., Saint Petersburg, Russia). During recording, the stimulation program continuously sent to the Mitsar system triggers to track precisely all event onsets of each trial. These triggers where received by the Mitsar system as a logic signal, synchronized with the EEG stream and recorded as a supplementary data channel.

8.8.4 Preprocessing

Data were filtered in the 1-40Hz band-pass region using an order four Butterworth FIR filter with linear phase response in the band-pass region. Ocular artifacts were extracted using the SOBI algorithm (Belouchrani et al., 1993) available in the EEGLAB toolbox (Delorme and Makeig, 2004). One EOG source corresponding to eye-blinks was suppressed for each subject. It was manually selected using both the temporal shape of the source and its topography. All other artifacts were left into the signal, so as to approximate the conditions of on-line analysis of EEG data acquired during BCI operation.

8.8.5 Analysis in the Sensor Space

The analysis in the sensor space is the traditional analysis of the signal as recorded at each electrode. We are interested in the analysis of the error vs. correct trials. We performed both the analysis of the event-related potential (ERP: both time- and phase-locked: Lopes Da Silva, 2005 b) and of the event-related synchronization (ERS: time-locked, but not necessarily phase-locked: Pfurtscheller and Lopes da Silva, 2004). ERPs were analyzed contrasting the average potential obtained from each subject at each electrode and time-sample. ERS were analyzed contrasting the average time-frequency map obtained on each trial from each subject at each electrode. In order to compute ERS we employed a multi-tapering Hanning sliding window (frequency dependent, with the taper equal to 4 cycles for each frequency) over the 2-32Hz band using a 1Hz step, as implemented in the Fieldtrip software (Oostenveld et al., 2011). ERS were computed on time window [-0,5s 1,2s] using a time step of 0,03s and a baseline defined as [-1s 0s] pre-stimulus.

The statistical analysis in the sensor space for contrasting “error” vs. “correct” trials needs to be performed for each electrode, discrete frequency and time segment in the case of ERS and for each electrode and time segment for ERP data. In order to account for the extreme multiple-comparison nature of the test we employed a permutation strategy. The test chosen is a slight modification of the supra-threshold cluster size permutation test originally proposed for neuroimaging data by Holmes et al. (1996). Here the statistic is not the supra-threshold cluster size, but the supra-threshold cluster intensity, defined as the sum of the t-values within the supra-threshold clusters. As compared to the test described by Holmes et al. (1996) such a statistic is influenced not only by the spatial extent of the clusters, but also by the strength of the effect. The test is sensitive to effects that are contiguous in space (adjacent

electrodes), frequency and time, in line with physiological considerations. The family-wise error rate for multiple comparisons was set to 0.05, meaning that the probability of falsely rejecting even only one hypothesis is less than 0.05. All permutation tests were approximated by the use of 5000 random permutations.

8.8.6 Analysis in the Source Space

As we have seen a spatial filter computes a weighted sum (linear combination) of the signal obtained at each electrode, potentially isolating delimited dipolar sources from each other. We apply here the method introduced above adapting it to ERP data. Our goal is to separate the source of the Ne (ERP) and the source for the theta ERS. We need to separate them one from the other, but also from background EEG activity. For our purpose we need to include in the diagonalization set matrices holding a) the spatial structure of the ERP component, b) the spatial structure of the ERS component, as well as c) the spatial structure of the spontaneous EEG oscillations and persistent artifacts such as lateral and horizontal eye movements, jaw muscle contractions, etc. For (a) and (b) we compute the relevant covariance matrices both on error trials and correct trials so to exploit variations of source energy between the two conditions (table 1). We define an exactly determined BSS model, that is to say, we estimate as many sources (M in the formula above) as electrodes (N=M=31). For the ERP components (a) we estimate the covariance matrix of the average ERP in the three time windows were the ERP analysis in the sensor space revealed significant results (see next section). Covariance matrices were separately computed for error and correct conditions, providing 3x2=6 matrices. *These six matrices provide unique source energy profile about ERP that have different potential in error vs. correct trials*. For the ERS component (b) we estimate the averaged covariance matrix in the time-frequency region were the sensor space analysis revealed significant results (see next section). These matrices were computed as the covariance matrices of the EEG filtered in the frequency band of interest. Again, matrices were computed separately for error and correct conditions, providing two additional matrices. *These two matrices provide unique source energy profile about ERS that display different power in the theta band in error vs. correct trials.* Notice that matrices for the ERP and the ERS components are substantially different: for the ERP components EEG trials are averaged before computing the covariance matrix (thus only both time-locked and phase-locked signals are preserved), while for the ERS components trials are averaged only after computing covariance matrices on single-trial data (thus non-phase-locked signal are preserved as long as they are time-locked). To separate possible sources of ERP and ERS from spontaneous EEG oscillations and artifacts (c) we include in the set all co-spectral matrices (Bloomfield, 2000) of the signal during the fixation cross sequence in the frequency range 2-20Hz using a frequency step of 2Hz, providing 10 additional matrices. *These latter 10 matrices provide unique source energy profile to separate all spontaneous sources having non-proportional power spectrum* (table 1). In summary, our BSS algorithm jointly diagonalizes a total of 18 matrices. For solving the approximate joint diagonalization we employ the iterative algorithm proposed by Tichavsky and Yeredor (2009), which is fast and in our long-lasting practice has proven robust.

Once estimated the 31 sources, they were inspected analyzing their ERP, ERS, topographies and the mutual information criterion between the source and the error class (Grosse-Wentrup and Buss, 2008). Meaningful sources were localized in a standard brain using the sLORETA inverse solution (Pascual-Marqui, 2002) as implemented in the LORETA-Key software. This software makes use of revisited realistic electrode coordinates (Jurcak, Tsuzuki and Dan, 2007) and the head model (and corresponding lead-field matrix) produced by Fuchs et al. (2002), applying the boundary element method on the MNI-152 (Montreal neurological institute, Canada) template of Mazziotta et al. (2001). The sLORETA-key anatomical template divides and labels the neocortical (including hippocampus and anterior cingulate cortex) MNI-152 volume in 6239 voxels of dimension 5 mm^3, based on probabilities returned by the Demon Atlas (Lancaster et al., 2000). The co-registration makes use of the correct translation from the MNI-152 space into the Talairach and Tournoux (1988) space (Brett et al., 2002). Source localization was conducted on each participant separately, normalized to unit global current density (the input of the inverse solution is a vector estimated by BSS up to a scale indeterminacy) and summed up over participants in the brain space.

8.8.7 Classification of single trials

For classifying single trials, data were band-pass filtered using an order four Butterworth FIR filter with linear phase response between 1-10Hz for the ERP component and 4-8Hz for the ERS component. Data were then spatially filtered using the results of the BSS analysis. Only samples corresponding to 250-750ms were kept. For the ERP component we used the temporal signal down-sampled at 32Hz, providing 16 samples (features) for the classification. For the ERS component we used the square of the temporal signal (power) dawn-sampled at 32Hz, providing 16 samples (features) for the classification as well. This procedure assigns to each component equal chance for classification. As a classifier we employed a LDA (linear discriminant analysis). One hundred random cross-validations were performed with the classifier trained on a randomly selected set containing 80% of the data (both errors and corrects) and then tested on the remaining data.

8.9 Results

8.9.1 Behavioral results

All subjects performed the task with a convenient error-rate, with mean (sd) = 22.2 (4)% and a quasi-equal repartition of expected and unexpected errors, with mean (sd) = 10.4 (4.3)% and 11.8(3)%, respectively. Reaction time was higher for error trials as compared to correct trials in 80% of the subjects (all t-tests with $p<0.05$). The maximum number of digits to memorize for each subject was highly variable, ranging from 4 to 10, with mean (sd) = 6.5

(1.37). These results demonstrate that our presentation software succeeded in equalizing the cognitive load across subjects, despite the great inter-subject variability of digit memory span.

8.9.2 Sensor Space Analysis

The ERP in the error trials differed from the correct trials in three time windows with different timing and/or electrode location (Fig. 8.3). A significant positivity for errors was found at time window [320ms 400ms] at electrode Cz ($p<0.01$), a significant negativity for errors at time window [450ms 550ms] at clustered electrodes Fz, FCz, Cz ($p<0.01$) and a significant positivity for errors at time [650ms 775ms] at clustered electrodes Fz, FCz ($p = 0.025$).

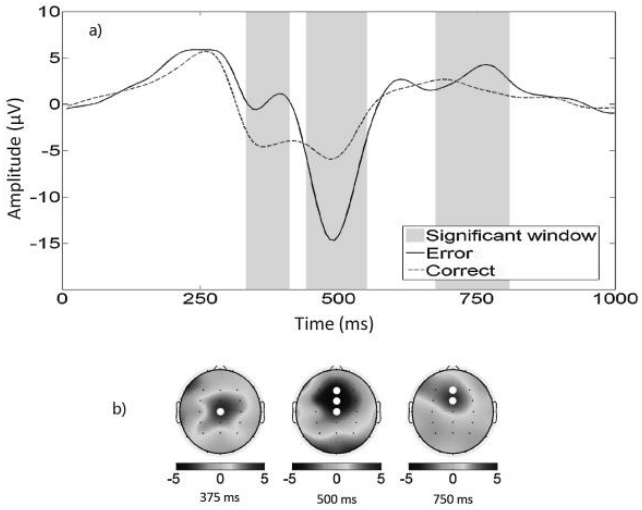

Figure 8.3 : (a): grand average (N=19) ERP for correct (pointed line) and error (solid line) trials. Time windows where the difference in amplitude between the two conditions is significant (grey panels) and (b) scalp topographies of t-values computed within the three significant windows. White disks show the significant clustered electrodes.

An ERS (power increase as compared to baseline) could be seen in the theta band in both correct and error feedback at fronto-midline locations. This synchronization unfolds from around 250ms to 600ms post-stimulus. In some subject it goes up to more than 200% of power increase for error trials. Albeit present in both conditions, this ERS is significantly more intense for error trials as compared to correct ones (Fig. 8.4) in the frequency band pass region 5-8Hz and time window [350ms 600ms] post-stimulus over the clustered electrodes Fz and FCz ($p = 0.015$).

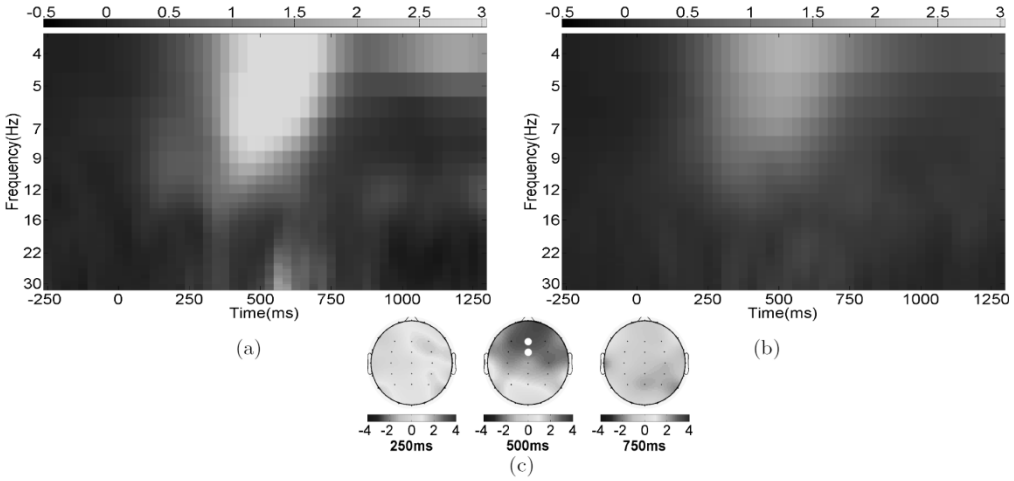

Figure 8.4: Grand average (N=19) ERS averaged at electrodes (Fz, FCz, Cz, CPz) for error (a) and correct (b) trials. (c): topographic maps of t-values averaged over the theta band and time window [350ms 600ms]. White disks show the significant clustered electrodes.

8.9.3 Source Analysis

BSS analysis revealed two uncorrelated sources with variable sensitivity and specificity, however clearly responsible one for the ERP findings and one for the ERS findings. The source responsible for the ERP differences between error and correct trials, to which hereafter we will refer to as the "Ne source", was significantly different in error vs. correct trials in two time windows, with a first negative peak at time window [460ms 540ms] ($p < 0.01$) and a positive peak at time [750ms 830ms] ($p = 0.015$). The grand-average ERP of this source computed separately for error and correct trials is displayed in Fig. 8.5a. In Fig. 8.5b it is displayed the same grand average ERP when computed using the spatial filter of the source responsible of the ERS differences between error and correct trials, to which hereafter we will refer to as the "theta source"; although differences in amplitude exist also for this latter source, they are not significant.

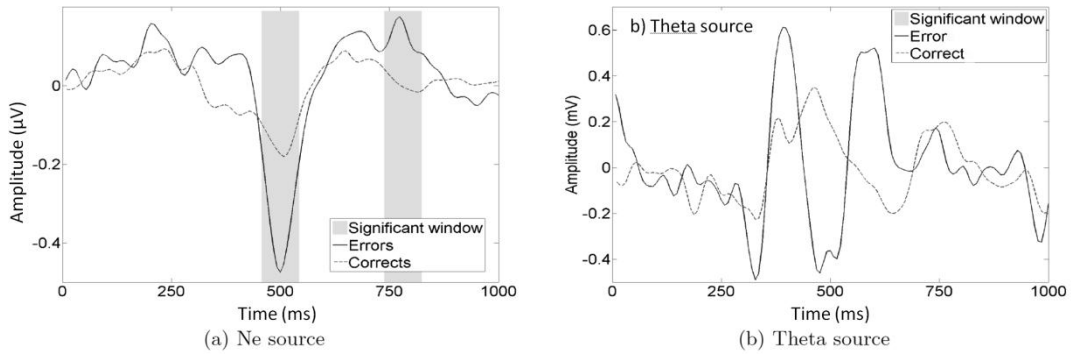

Figure 8.5: Grand averaged (N=19) of the ERP generated by the Ne source (a) and by the theta source (b) for error (solid line) and correct (pointed line) trials. Time windows were the difference in amplitude between the two conditions is significant are highlighted by grey panels.

On the other hand the theta source power increase was significant in frequency band-pass region [5Hz 8Hz] for time window [300ms 600ms] ($p<0.01$). The ERS generated by this source is shown in Fig. 8.6b. In Fig. 8.6a it is displayed the same ERS when computed using the spatial filter of the Ne source instead; the ERS in this case disappears. These results suggest that the Ne source and the theta source correspond to separate phenomena generated by different brain structures with different dynamics. The source responsible for the ERS (theta source) appears more specific.

We can now illustrate the advantage brought upon from the BSS analysis with these data. Compare Fig. 8.5a to 8.3 and Fig. 8.6 to 8.4. *Although in both cases results in the sensor space are computed for the optimal cluster of electrodes, in both cases it is clear that working in the source space allows a better sensitivity and specificity: in both cases the difference between the error and correct trials is highlighted.*

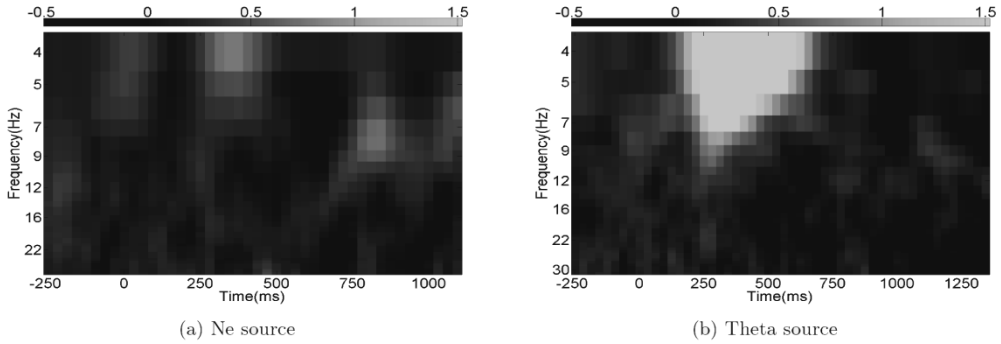

(a) Ne source (b) Theta source

Figure 8.6: Grand average (N=19) of the ERS generated by the Ne source (a) and by the theta source (b) for error trials.

8.9.4 Source localization

The BSS source responsible for the ERP (Ne source) difference between correct vs. error trials was localized by sLORETA in the anterior cingulate gyrus (BA 24). The BSS source responsible for the ERS (theta source) was localized close to the supplementary motor area (BA 6) (Fig. 8.7). Keeping in mind the approximation of a source localization method applied on a standard head model, these anatomical results are in line with results reported by previous studies (Gehring and Willoughby, 2002; Herrmann et al., 2004; Nieuwenhuis et al., 2003).

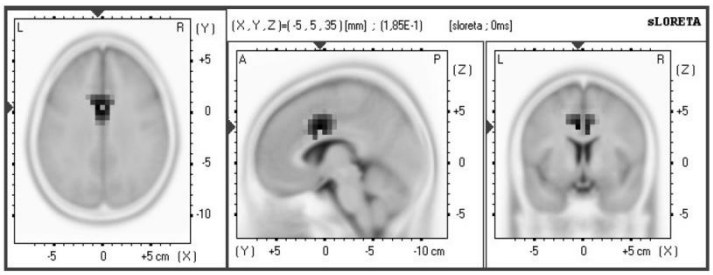

(a)

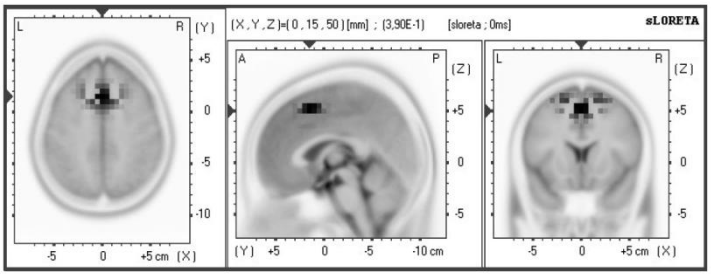

(b)

Figure 8.7: (a) Ne source sLORETA localization. The source is localized in BA 32. (b) Theta source sLORETA localization. The source is localized in BA 6. For each image, from left to right are the axial, sagittal and coronal views across the maximum. The images (a) and (b) are scaled to their own maximum. The activity is color-coded with black representing the maximum and transparent representing zero. Legend: A=Anterior;P=Posterior; S=Superior; I=Inferior; L=Left; R=Right.

8.9.5 Error Expectation

We then studied the impact of the error expectation on the two identified sources identified (Ne and ERS). Each trial could outcome one out of four results: unexpected errors (UE), expected errors (EE), expected corrects (EC), unexpected corrects (UC). Since most subjects reported no trials from the UC condition we only studied the first three outcomes. Only subjects providing at least four trials for each condition were kept. Three further subjects were therefore excluded from this analysis. For each component a one-way repeated-measure ANOVA with factor "outcome feedback" at three levels was applied i) to the temporal signal averaged over time window [450ms 520ms] for the Ne source and ii) to the power signal filtered between 5 and 8Hz and averaged over significant time window [300ms 600ms] for the theta source. For the Ne source no significant result was found. For the theta source the means of the three outcomes were not all equal ($F = 4.75$; $p = 0.0138$). All pair-wise post-hoc tests corrected by Bonferroni method showed that the ERS engendered by this source is in this relationship: ERS(UE)>ERS(EE)>ERS(EC), with both inequality signs indicating a significant difference ($p<0.05$).

8.9.6 Classification of single trials

The Ne source alone leads to better accuracy in classifying error trials as compared to the theta source alone ($p < 0.01$). The theta source leads to better accuracy for classifying correct trials ($p = 0.028$). These corroborate the conclusion that the ERP and ERS represent

different phenomena of the ErrP. When looking at the average classification rate (Te+Tc)/2, with Te the classification rate of error trials and Tc the classification rate of correct trials, one see that the use of both components leads to better results for 14 subjects out of 19. The use of both components increases the mean classification rate on the 19 subjects from 67% up to 71%. We performed a repeated measure two-way ANOVA with factor "type" (error vs correct) and "feature" (Ne source ERP, theta source ERS, both). It revealed a main effect on the "type" factor ($p < 0.01$) with correct trials being better classified than error trials and a "type" x "feature" interaction ($p = 0.013$), demonstrating that the use of both the ERP and the ERS feature in the source space improves the performance of single trial classification. It should be noticed that with a total of 72 trials per subject, training set included only a mean of 17 single trials for the error condition, thus the classification task for this data set is hard since the training sets include very few examples of error trials.

Knowing that the error expectation has an influence on the theta ERS we have looked at classification results for expected and unexpected errors, for the theta ERS components and the Ne ERP components. Classification performance is higher for unexpected errors (mean Te=62%) than for expected errors (mean Te=47%) ($p = 0.011$) when using the theta ERS component. On the other hand, results are equivalent (mean Te=63% for unexpected errors and mean Te=64% for expected errors) using the Ne ERP component for classification. Thus, classification using the theta ERS component performs poorly on error trials only for expected errors. As a consequence, in the case of a system where errors are unexpected, the classification using the theta ERS component as compared to using the Ne ERP component would allow similar results for error trials and better results for corrects trials, leading to a better average classification accuracy.

8.10 Conclusions and Discussion

We have described a blind source separation approach requiring only estimation of second-order statistics of data, that is, covariance matrices. The method, which is well grounded on current theory of volume conduction, is consistently solved by means of approximate joint diagonalization of a set of covariance matrices, whence the name (AJDC). AJDC is simple, fast and flexible, allowing explicit modeling of physiological and experimental a-priori knowledge. We have argued that the success of the source separation depends solely on

- An appropriate choice of covariance matrices to form the diagonalization set;
- Their appropriate estimation.

To fulfill the first requirement we have provided guidance for the analysis of continuously recorded EEG, event-related (de)synchronizations (ERS/D) and event-related potentials (ERP). While studies for the first two cases are already available and well established, we have here presented for the first time the use of AJDC for ERD. We have conducted a source analysis by means of BSS of the feedback ErrP in high cognitive load

conditions. In this experiment we have used conditions that resemble those one can find on real BCI experiments. Our results showed that the feedback-related potential observed here shares the same characteristics as the FRN observed in gambling tasks and the ERN observed in reaction-time tasks. Indeed all three error potentials are notably characterized by a negative deflection generated by the dorsal-ACC, but with different time of activation. A sharp analysis in the source space by means of approximate diagonalization of covariance matrices has allowed the identification of three main components accounting for the differentiation between error and correct trials. Two temporal (ERP) characteristics were identified: a first sharp negativity (Ne) and a broad positivity (Pe). One frequential (ERS) characteristic was identified as theta ERS at the same time that the Ne. This observation is in accordance with previous findings (Luu, Tucker and Makeig, 2004; Trujillo and Allen, 2007) which also pointed to the implication to oscillations in the theta band as an indicator of response error related potentials. Luu Tucker and Makeig (2004) reported that the theta band (4-7Hz) is responsible for most variability of the ERN (57%) meanwhile Trujillo and Allen (2007) reported a power increase in the theta band at a time course similar to the Ne for erroneous responses. In this paper we have observed that the ErrPf is characterized by an important ERS in the theta band. This ERS seems to occur at the same time as the negative evoked potential. This observation leads to the question of the independence of these two components. Indeed, even if they occur simultaneously they may represent different manifestation of the same neuronal process. Blind source separation coupled with source localization (sLORETA) has allowed the identification of two spatially distinct sources, one accounting for the temporal component (BA24) and one for the frequency component (BA6). Statistical analysis at source level validated this separation with a significant temporal activity only for the first source exhibiting a significant ERP at the time of Ne and Pe and a significant ERS only for the second source in the theta band. The fact that these two sources are uncorrelated and spatially segregated suggests that these two phenomena do not reflect the same neuronal process. This point is of great interest for BCI applications and for the on line detection of the ErrPf since they may therefore provide independent information for classification. In fact, up to now in BCI only the negative wave (Ne) has been used as a feature for classifying the ErrPf. Our results suggest that one could use both the ERP and the ERS component. Indeed our classification results showed that the theta ERS brings independent information and allows better classification results (as compared with using the ERP alone). It has to be noted that while the Ne was clearly identifiable in all subjects, the Pe was not strong enough to be clearly identified in some subjects. This might explain why our BSS approach has not been successful in finding separated sources for the Pe peaks (poor signal to noise ratio and/or high inter-individual variability).

Interestingly, we have found that the expectation of the outcome has a direct impact on the theta ERS, but not on the Ne; the more the error is expected the weaker is the theta ERS. To our knowledge no such effect has been reported so far. We conclude that the error-related potential may depend on two factors: the value of the observation (erroneous or correct) and the expectation of the outcome. Thus, the error-related potential may be the combination of two reactions, one to the error and the other to the surprising character of the observation. Further studies may now try to investigate this new aspect of the error related potential and try

to determine if these two components are physiologically separated or interlaced. Within the frame of a BCI application, the more accurate the BCI is, the more unexpected the error will be. Classification results showed that, when using theta component, performance is higher for unexpected errors as compared to expected errors. If the subject is concentrated and performs well the task, the occurrence of an error will be less expected, since it would result mainly from a nuisance such as an artifact decreasing the signal-to-noise-ratio. Under these circumstances the theta ERS component will be more efficient in detecting errors coming directly from the interface. In order to improve ErrP recognition in a real BCI system the performance of the system should be maximized, so that the ErrP can be more easily detected. We conclude that the theta ERS will be stronger for high performance BCIs and therefore that the error can be more easily detected for high performance BCI. This fact should be taken into consideration in ensuing attempts to integrate a control loop based on ErrP detection in a BCI. More in general, the error potential should not be seen as a panacea for correcting BCI operation errors, since a high number of errors will lead to a poor detection of ErrP.

In conclusion, the AJDC method proves at the same time flexible and powerful. We hope that it turns out useful for extracting meaningful information to be used in the studies at the cross road of music and brain electrophysiology.

8.11 Questions

1) What are the physical generators of brain electric fields recordable from the scalp?

2) Why a linear mixing model is a good approximation for the genesis of observable scalp potentials?

3) What is the relation between the mixing matrix and the demixing matrix?

4) List the main sources of instrumental, biological and environmental noise affecting EEG recordings

5) What is an error-related potential (ErrP)?

6) The ERS associated to the ErrP is temporally related to a positive or to a negative evoked potential?

7) What are the advantages of a source-level analysis via blind source separation as compared to a sensor-level analysis?

8) Why the blind source separation method is said to be “blind”?

9) Create an experimental design where a blind source separation method exploiting source non-stationary would be appropriate for data analysis.

10) Why error-related potentials are of interest in the field of brain-computer interface?

8.12 References

Afsari B (2008) Sensitivity analysis for the problem of matrix joint diagonalization, SIAM Journal on Matrix Analysis and Applications, 30(3) 1148–1171.

Aïssa-El-Bey A, Abed-Meraim K, Grenier Y, Hua Y (2008) A general framework for second order blind separation of stationary colored sources. Signal processing, 88(9), 2123-2137.

Ans B, Hérault J. Jutten C. (1985) Adaptive Neural Architectures: Detection of Primitives. In : Proc. COGNITIVA, 593-597.

Bell AJ, Sejnowski TJ. (1995) An Information-Maximization Approach to Blind Separation and Blind Deconvolution. Neural Comput, 7, 1129-1159.

Belouchrani A, Amin MG. (1998) Blind Source Separation Based on Time-Frequency Signal Representations. IEEE Trans Signal Process46(11), 2888-2897.

Belouchrani A, Abed-Meraim K, Cardoso JF, Moulines E (1997) A blind source separation technique using second order statistics', IEEE Trans. on Signal Processing, 45(2), 434-444.

Bloomfield P. Fourier Analysis of Time Series. New York: John Wiley & Sons, 2000.

Bollon JM, Chavarriaga R, Millan J, Bessiere P(2009) EEG error-related potentials detection with a Bayesian, Proceedings of the 4th International IEEE EMBS Conference on Neural Engineering, 702-705.

Brett M, Anton J-L, Valabregue R, Poline J-B (2002) Region of interest analysis using an SPM toolbox [abstract] presented at the 8th International Conference on Functional Mapping of the Human Brain, June 2–6, 2002, Sendai, Japan. Available on CD-ROM in NeuroImage 16(2).

Cardoso J-F (1998) Blind Signal Separation: Statistical Principles. IEEE Proc., 9(10), 2009-2025.

Cardoso JF, Souloumiac A (1993) Blind beamforming for non-Gaussian signals. IEE Proc-F (Radar and Signal Process), 140(6), 362-370.

Chatel-Goldman J, Congedo M, Phlypo R (2013) Joint BSS as a natural analysis framework for EEG-hyperscanning, in press

Comon P (1994) Independent component analysis, A new concept? Signal Processing 36(3), 287–314.

Comon P, Jutten C (2010) Handbook of Blind Source Separation: Independent component analysis and applications. Academic Press, London.

Congedo C, Gouy-Pailler C, Jutten C (2008) On the blind source separation of human electroencephalogram by approximate joint diagonalization of second order statistics. Clin Neurophysiol, 119(12), 2677-2686.

Congedo M, John ER, De Ridder D, Prichep L (2010) Group Independent Component Analysis of Resting-State EEG in Large Normative Samples, International Journal of Psychophysiology, 78, 89-99.

Congedo M, Phlypo R, Chatel-Goldman J (2012) Orthogonal and Non-Orthogonal Joint Blind Source Separation in the Least-Squares Sense, 20th European Signal Processing Conference (EUSIPCO), Aug 27-31, Bucharest, Romania, 1885-9.

Congedo M, Phlypo R, Pham D-T (2011) Approximate Joint Singular Value Decomposition of an Asymmetric Rectangular Matrix Set, IEEE Transactions on Signal Processing 59(1), 415-424.

Darmois G (1953) Analyse générale des liaisons stochastiques. Rev Inst Inter Stat, 21, 2-8.

Delorme A, Makeig S (2004) EEGLAB: an open source toolbox for analysis of single-trial EEG dynamics including independent component analysis. J. Neurosci. Methods, 134(1), 9-21.

Falkenstein M, Hohnsbein J, Hoormann J (1991) Effects of crossmodal divided attention on late ERP components. II. Error processing in choice reaction tasks. Electroencephalography and Clinical Neurophysiology 78, 447–455.

Falkenstein M, Hoormann J, Christ S, Hohnsbein J (2000) ERP components on reaction errors and their functional significance: a tutorial. Biol Psychol, 51(2-3), 87-107.

Farquhar J, Hill NJ. (2013) Interactions between pre-processing and classification methods for event-related-potential classification : best-practice guidelines for brain-computer interfacing. Neuroinformatics, 11(2),175-92.

Ferrez PW, Millan JR (2005) You are wrong! Automatic detection of interaction errors from brain waves. In Proceedings of the 19th International Joint Conference on Artificial Intelligence.

Fuchs M, Kastner J, Wagner M, Hawes S, Ebersole JS (2002) A standardized boundary element method volume conductor model. Clinical Neurophysiology, 113(5), 702-712.

Gehring WJ, Goss B, Coles MGH, Meyer DE, Donchin E (1993) A neural system for error detection and compensation. Psychol. Sci., 4(Suppl 6):385{390, 1993.

Gehring WJ, Willoughby AR (2002) The medial frontal cortex and the rapid processing of monetary gains and losses. Science, 295(5563), 2279-2282.

Gentsch A, Ullsperger P, Ullsperger M (2009) Dissociable medial frontal negativities from a common monitoring system for self-and externally caused failure of goal achievement. Neuroimage, 47(4), 2023-2030.

Gouy-Pailler C, Congedo M, Brunner C, Jutten C, Pfurtscheller G (2010), Nonstationary brain source separation for multiclass motor imagery, IEEE Transactions on Biomedical Engineering 57(2), 469-78.

Grosse-Wentrup M, Buss M (2008) Multiclass common spatial patterns and information theoretic feature extraction. IEEE Trans. Biomed. Eng., 55(8), 1991-2000.

Hérault J, Jutten C. (1986) Space or time adaptive signal processing by neural network models. Proc Int Conf Neural Netw Computing, Snowbird (Utah), 151, 206-211.

Herrmann M.J. Römmler J, Ehlis AC, Heidrich A, Fallgatter AJ (2004) Source localization (LORETA) of the error-related-negativity (ERN/Ne) and positivity (Pe). Cognitive Brain Research, 20(2), 294-299.

Holmes AP, Blair R C, Watson JDG, Ford I (1996) Non-Parametric Analysis of Statistic Images From Functional Mapping Experiments. Journal of Cerebral Blood Flow and Metabolism, 16, 7-22.

Jurcak V, Tsuzuki D, Dan I (2007) 10/20, 10/10, and 10/5 systems revisited: their validity as relative head-surface-based positioning systems. Neuroimage, 34(4), 1600-1611.

Jutten C, Hérault J. Blind separation of sources, Part 1: an adaptive algorithm based on neuromimetic architecture. Signal Process 1991; 24(1): 1-10.

Kopřivová J, Congedo M, Horáček J, Praško J, Raszka M, Brunovský M, Kohútová B, Höschl C (2011) EEG source analysis in obsessive–compulsive disorder, Clinical Neurophysiology 122(9), 1735-1743.

Lancaster JL, Woldor MG, Parsons LM, Liotti M, Freitas CS, Rainey L, Kochunov PV, Nickerson D, Mikiten SA, Fox PT (2000) Automated Talairach atlas labels for functional brain mapping. Human brain mapping, 10(3), 120-131.

Lopes da Silva F (2005) Event Related Potentials: Methodology and Quantification. In: Electroencephalography. Basic Principles, Clinical Applications, and Related Fields. Niedermeyer E and Lopes da Silva F. (Eds), 5th ed., New York: Lippincott Williams & Wilkins, 991-1001.

Lopes da Silva F, Van Rotterdam A (2005) Biophysical Aspects of EEG and Magnetoencephalogram Generation. In: Electroencephalography. Basic Principles, Clinical Applications, and Related Fields. Niedermeyer E and Lopes da Silva F. (Eds), 5th ed., New York: Lippincott Williams & Wilkins, 107-125.

Luu P, Tucker DM, Makeig S (2004) Frontal midline theta and the error-related negativity: neurophysiological mechanisms of action regulation. Clin Neurophysiol, 115(8), 1821-1835.

Matsuoka K, Ohya M, Kawamoto M (1995) A neural net for blind separation of nonstationary signals. Neural Netw, 8(3), 411-419.

Mazziotta J, Toga A, Evans A, Fox P, Lancaster J, Zilles K, Woods R, Paus T, Simpson G, Pike B, et al. (2001) A probabilistic atlas and reference system for the human brain: International consortium for brain mapping (icbm). Philosophical Transactions of the Royal Society of London. Series B: Biological Sciences, 356(1412), 1293-1322.

Miltner WHR, Braun CH, Coles MGH (1997) Event-related brain potentials following incorrect feedback in a time-estimation task: Evidence for a generic neural system for error detection. Journal of Cognitive Neuroscience, 9(6), 788-798.

Molgedey L, Schuster, HG Separation of a Mixture of Independent Signals using Time Delayed Correlations. Phys Rev Lett 1994; 72: 3634-3636.

Niedermeyer E (2005 a) The Normal EEG of the waking Adult. In: Electroencephalography. Basic Principles, Clinical Applications, and Related Fields. Niedermeyer E and Lopes da Silva F. (Eds), 5th ed., New York: Lippincott Williams & Wilkins, 167-191.

Niedermeyer E (2005 b) Sleep and EEG. In: Electroencephalography. Basic Principles, Clinical Applications, and Related Fields. Niedermeyer E and Lopes da Silva F. (Eds), 5th ed., New York: Lippincott Williams & Wilkins, 193-207.

Nieuwenhuis S, Yeung N, Van Den Wildenberg W, Ridderinkhof KR (2003) Electrophysiological correlates of anterior cingulate function in a go/no-go task: E_ects of response conict and trial type frequency. Cognitive, Affective, & Behavioral Neuroscience, 3(1), 17-26.

Nunez PL, Srinivasan R. (2006) Electric Field of the Brain, 2nd ed., New York: Oxford Univ Press.

Oostenveld R, Fries P, Maris E, Schoffelen JM (2011) Fieldtrip: open source software for advanced analysis of meg, eeg, and invasive electrophysiological data. Computational Intelligence and Neuroscience, 1, ID 156869.

Pascual-Marqui R D (2002) Standardized Low-Resolution Brain Electromagnetic Tomography (sLORETA): Technical details, Meth. Find. Exp. Clin. Pharma, 24D, 5-12.

Pham D-T (2002) Exploiting source non stationary and coloration in blind source separation. Digital Signal Process, 1, 151-154.

Pham D-T, Cardoso J-F. (2001) Blind Separation of Instantaneous Mixtures of Non Stationary Sources. IEEE Trans Signal Process , 49(9), 1837-1848.

Pfurtscheller G (1981) Central beta rhythm during sensorimotor activities in man. Electroencephalography and clinical Neurophysiology, 51(3), 253-264.

Pfurtscheller G, Lopes da Silva F (1999). Event-related eeg/meg synchronization and desynchronization: basic principles. Clinical Neurophysiology, 110(11), 1842-1857.

Sarvas J. (1987) Basic Mathematical and Electromagnetic Concepts of the Biomagnetic Inverse Problem. Phys Med Biol, 32(1), 11-22.

Souloumiac A. (1995) Blind Source Detection and separation using second order nonstationarity. In Proc ICASSP, 1912-1915.

Speckmann E-J, Elger CE (2005) Introduction to the Neurophysiologicalal Basis of the EEG and DC Potentials. In: Electroencephalography. Basic Principles, Clinical Applications, and Related Fields. Niedermeyer E and Lopes da Silva F. (Eds), 5th ed., New York: Lippincott Williams & Wilkins, 17-29.

Steinhauser M Kiesel A (2011) Performance monitoring and the causal attribution of errors. Cognitive, Affective, & Behavioral Neuroscience, 1-12.

Steriade M (2005) Cellular Substrates of Brain Rhythms. In: Electroencephalography. Basic Principles, Clinical Applications, and Related Fields. Niedermeyer E and Lopes da Silva F. (Eds), 5th ed., New York: Lippincott Williams & Wilkins, 31-83.

Talairach J, Tournoux P (1988) Co-planar stereotaxic atlas of the human brain: 3-dimensional proportional system: an approach to cerebral imaging. Thieme.

Tichavsky T, Yeredor A (2009), Fast Approximate Joint Diagonalization Incorporating Weight Matrices, IEEE Tr. on Signal Processing, 57(3), 878-89.

Tong L, Inouye Y, Liu RW (1993) Waveform-Preserving Blind Estimation of Multiple Independent Sources IEEE Trans Signal Process, 41(7), 2461-2470.

Trujillo LT, Allen JJB (2007) Theta EEG dynamics of the error-related negativity. Clinical Neurophysiology, 118(3), 645-668.

Van Der Loo E. Congedo M, Plazier M, Van De Heyning P, De Ridder D (2007) Correlation Between Independent Components of Scalp EEG and Intra-Cranial EEG (iEEG) Time Series, International Journal of Bioelectromagnetism, 9(4), 270-275.

Yeredor A (2010) Second order Methods based on color. In Comon P and Jutten C (Eds.) Handbook of Blind Source Separation. Indipendent Component Analysis and Application, Academic Press, Paris.

Westfall P, Young S (1993) Resampling-based Multiple Testing: Examples and methods for p-value adjustment. John Wiley & Sons, New York.

White D, Congedo M, Ciorciari J, Silberstein R (2012) Brain oscillatory activity during spatial navigation: Theta and gamma activity link medial temporal and parietal regions, Journal of Cognitive Neuroscience 24(3), 686-697.